Enhanced phosphate adsorption on Ca-Mg-loaded biochar derived from tobacco stems

Man Yi and Yucheng Chen

ABSTRACT

Tobacco stems were used as precursors to prepare biochars (YGs) and develop Ca-Mg-loaded biochars (CMYGs) to enhance phosphate adsorption from aqueous solutions. Some influencing factors, such as pH, adsorption time, temperature, and structure characterization, were investigated. Fourier transform infrared (FTIR) spectra and X-ray diffraction (XRD) patterns showed several new peaks, indicating that $Mg(OH)_2$ and MgO have been present on the surface of the CMYGs. The adsorption could reach equilibrium in 100 min reaction. The equilibrium data were well described by the Langmuir and Freundlich model. After five recycles, the phosphate removal capacity of CMYGs biochar retained over 50%. Moreover, the XRD and FTIR analyses showed that the phosphate sorption mechanisms involved surface electrostatic attraction, inner-sphere complexation and precipitation reactions. Overall, the soaking method could be used to effectively load Mg^{2+} onto the surface of YGs. The CMYGs synthesized at 750 °C is a promising adsorbent for phosphate removal with a high adsorption capacity for phosphate-polluted wastewater.

Key words | adsorption isotherms, adsorption kinetics, biochar, desorption, phosphate, tobacco stems

Man Yi
Yucheng Chen (corresponding author)
Chongqing Engineering Research Center of Rural Cleaning,
Chongqing 400716,
China
and
College of Resources & Environment,
Southwest University,
Chongqing 400715,
China
E-mail: *chenyucheng@swu.edu.cn*

INTRODUCTION

Phosphate (P) compounds, as the basic components of plant and animal proteins, are essential nutrients for all organisms (Cordell *et al.* 2011; Elser & Bennett 2011). However, phosphate is also the main limiting factor to lake eutrophication. Phosphate concentrations below 0.02 mg/L can lead to uncontrolled growth of organisms, especially algae. Such uncontrolled growth can cause reductions in water oxygen content and the production of toxins, particularly in shallow lakes, estuarine and coastal marine regions, leading to fish deaths and harm to aquatic ecosystems (Li *et al.* 2016b). In addition, the natural recovery of phosphate is inefficient because phosphate is converted into sedimentation over time and then released into the water again (Loganathan *et al.* 2014; Qiu *et al.* 2015). Hence, highly effective methods to remove phosphate from wastewater are needed. To date, physical, chemical, and biological purification and adsorption methods have been widely used in wastewater treatment to minimize phosphate ion concentrations (Fox *et al.* 2014; Melia *et al.* 2017). Among these methods, adsorption is a low-cost and high-efficiency method (Li *et al.* 2017) and has been widely considered for phosphate removal from wastewater (Jung & Ahn 2016; He *et al.* 2017; Yang *et al.* 2018).

Recently, biochar has been used as a potential adsorbent for pollutant recovery due to its beneficial properties including low cost, environmental friendliness, excellent stability, general safety and high porosity (Guo *et al.* 2014; Hou *et al.* 2016). As a result, research has focused on the application of biochar for phosphate recovery because of its strong sorption affinities and low material cost (Li *et al.* 2016b; Li *et al.* 2017).

However, the surfaces of biochars are predominantly net negatively charged, which confers them only negligible ability to absorb anionic pollutants (Li *et al.* 2016b). To improve the phosphate adsorption performance of biochar, cation-modified biochar has recently been developed (Zhou *et al.* 2013; Wan *et al.* 2017). Previous studies have developed new functional materials by loading cations, such as Fe-modified wheat straw (Zhou *et al.* 2013), Bi-modified cottonwood (Zhu *et al.* 2016), and Al-treated biochar (Zhang & Gao 2013), which have yielded phosphate removal percentages in the range of 84.65–99.3%. However,

doi: 10.2166/wst.2019.001

the feasibility of these cation-modification methods is strongly controlled by the cost of the metal salts and their environmental friendliness. Johnston and Rittmann (Rittmann *et al.* 2011) pointed out that aluminum and iron were toxic to the environment. Calcium and magnesium can be used as metal sources with many benefits because they are involved in chlorophyll formation in plants and are environmentally friendly; in addition, the metal salts are easily obtained in nature, and their alkaline character can neutralize acids and provide a suitable pH range for nutrient recovery (Zhang *et al.* 2012; Fang *et al.* 2014; Li *et al.* 2017). For instance, Li *et al.* (2017) prepared mesoporous MgO-modified sugarcane residue biochar with a maximum removal capacity of 398 mg/g for phosphate in swine wastewater (Li *et al.* 2017), and Yin & Kong (2014) used a calcium-rich attapulgite adsorbent for phosphate adsorption (Yin & Kong 2014). They had achieved high phosphorus removal rates, adopting calcium or magnesium modification individually. However, there were few studies about the adsorbent combined modification of calcium and magnesium. In addition, it is still unclear that whether a synergistic effect on phosphate adsorption exists between calcium and magnesium in the synthetic Ca-Mg-loaded biochar. Therefore, it is of great significance to investigate Ca-Mg-loaded biochar for phosphate recovery.

This research aimed to develop an inexpensive and efficient adsorbent for phosphate recovery. Firstly, biochar derived from tobacco stems was modified with calcium and magnesium. Then, the basic physicochemical properties of tobacco stem biochar (YGs) and Ca-Mg-loaded biochar (CMYGs) were characterized, and their phosphate removal efficiencies were compared. Lastly, the underlying mechanism was discussed.

MATERIALS AND METHODS

Materials

The tobacco stems used in this study were obtained from the tobacco-growing area in Banan District of Chongqing, China. The fresh tobacco stems were washed with deionized water to remove dirt and air-dried at room temperature for 1 week. Then, they were cut into 1–5 cm pieces, washed several times with tap water, dried in a furnace at 338 K for 24 h, and sealed in a container before use.

The phosphate stock solution was prepared by dissolving potassium dihydrogen orthophosphate (KH_2PO_4) powder in deionized water, and the desired solutions were prepared by diluting the phosphate stock solution. All of the chemical reagents used in the study were of analytical grade.

Biochar preparation and modification

The prepared tobacco stems were pyrolyzed at 350 °C, 550 °C, or 750 °C in a high-purity nitrogen gas (99.999%, limited oxygen) flow at 300 mL/min for 4 h in a furnace (GF11Q-B, Nanjing, China) with a heating rate of 5 °C/min. After cooling to ambient temperature, the pyrolyzed samples were crushed and sieved to obtain the desired particle size (40–80 mesh) using a fine-mesh mill (C-800Y, Zhejiang, China). Finally, the obtained biochar was washed with tap water until the pH level stabilized, dried in a vacuum oven at 358 K for 24 h and bottled (denoted YGs, s = 350, 550, and 750).

The CMYGs were generated through a pyrolysis and impregnation process. In this experiment, 10 g obtained biochar samples (YG350, YG550, or YG750) was dipped in 800 mL mixed solution, containing 400 mL $CaCl_2$ (2 mol/L) and 400 mL $MgCl_2$ (3 mol/L), which were then shaken at 180 rpm and 298 K for 24 h. After the reaction, the samples were washed with distilled water until the pH level stabilized, dried in a vacuum oven at 358 K for 24 h and stored in a tightly closed screw cap bottle (denoted CMYGs, s = 350, 550, and 750).

Test methods

Effect of the solution pH

To determine the effect of pH on the adsorption of YGs/CMYGs to phosphate, 1 g of YGs or CMYGs was weighted into 80 mL phosphate solution (50 mg/L), which were then shaken at 180 rpm (303 ± 0.5 K) for 24 h. The pH values (4–10) of the solutions were adjusted using a 0.1 mol/L HCl or 0.1 mol/L NaOH solution. Finally, the supernatants were filtered through a 0.45 μm cellulose acetate membrane, and the phosphate concentrations were determined by the standard method.

Dynamic characteristics

In this experiment, 1 g of YGs or CMYGs was added to 80 mL phosphate solution (50 mg/L), which were then shaken at 180 rpm (303 ± 0.5 K) for 24 h. The supernatant was collected at different time intervals. At specified time intervals (1, 3, 5, 10, 15, 20, 40, 70, 120, 170, 250 and

350 min), the flasks were removed, and the supernatants were immediately filtered through 0.45 μm microfiltration membranes to collect the filtrates. Then, the residual phosphate concentration in each filtrate was spectrophotometrically estimated by ammonium molybdate spectrophotometry; the absorbance at 700 nm was monitored by a UV-vis spectrophotometer (T6, Nanjing, China).

Adsorption isotherm

To examine the adsorption isotherm of the biochar, 1 g adsorbent was added into 80 mL phosphate solution with different initial concentration (10–100 mg/L). The flasks were placed in a thermostatic shaker at the desired temperature (298 ± 0.5, 303 ± 0.5 or 318 ± 0.5 K) and shaking rate (180 rpm) for 24 h. Finally, the supernatants were filtered through a 0.45 μm microfiltration membrane, and the phosphate concentrations were determined by the standard method.

Desorption experiment

For the desorption experiment, CMYGs (1 g) were exposed to phosphate at a concentration of 50 mg/L, and the adsorption capacity was calculated as described above. In this process, a complex of P-loaded biochar was achieved (denoted P-CMYGs). After adsorption, the P-loaded biochar was washed with deionized water to remove any unadsorbed phosphate and dried in an oven at 358 K. For desorption, the P-loaded biochar was added to a desorption reagent (pure water, 0.1 mol/L HCl, 0.1 mol/L NaOH or 0.1 mol/L NaCl) and shaken for 24 h, and the supernatant was separated and again detected to calculate the desorption amount.

Analysis methods

Characterization methods

The phosphate concentrations were determined by ammonium molybdate spectrophotometry (GB 11893–89) (Shi *et al.* 2011). The calcium and magnesium contents were determined by flame atomic absorption spectrophotometry (GB 11904-89). The YGs and CMYGs were analyzed with a Fourier transform infrared spectrometer (FTIR, Nicolet 6700, Neighborhood Company, USA), a Brunauer–Emmett–Teller surface area analyzer (BET, ASAP, Mike, USA), a field emission scanning electron microscope (SEM, SU8010, Hitachi, Japan), and an X-ray powder diffractometer (XRD, D8 ADVANCE, Brooke Company, Germany). The isoelectric point (pH_{pzc}) of the biochar was determined by the Babic batch method (Babic *et al.* 1999).

All of the experiments were performed three times, and the average values are reported. Additional analyses were conducted when two measurements had a difference greater than 5%.

Biochar adsorption

The adsorption capacity, q_e (mg/g), of the biochar for phosphate at equilibrium was calculated as follows:

$$q_e = \frac{(C_0 - C_e)V}{W} \tag{1}$$

where V (mL) is the volume of the phosphate solution; c_o and c_e (mg/L) represent the concentrations of phosphate at the initial and equilibrium time, respectively; and W (g) is the weight of the biochar.

Adsorption kinetics

In this study, the experimental data were simulated by pseudo-first-order, pseudo-second-order (Boparai *et al.* 2011; Bao *et al.* 2014) and intraparticle diffusion equations (Hou *et al.* 2016).

The linear pseudo-first-order equation can be expressed as follows:

$$\lg(q_e - q_t) = \lg q_e - k_1 \times \frac{t}{2.303} \tag{2}$$

The linear pseudo-second-order equation can be expressed as follows:

$$\frac{t}{q_t} = \frac{1}{k_2 q_e^2} + \frac{t}{q_e} \tag{3}$$

$$\text{Order: } h = k_2 \times q_e^2 \tag{4}$$

The particle diffusion equation can be expressed as follows:

$$q_t = k_p \times t^{0.5} + C \tag{5}$$

where t is the adsorption time (min); q_t and q_e are the amounts of phosphate (mg/g) adsorbed at time t and at equilibrium time, respectively; k_1, k_2 and k_p (mg/(g·min)) are the

rate constants; C is a constant related to the boundary layer thickness; and h is the initial adsorption rate (mg/(g·min)).

Adsorption isotherms

In this study, two types of isothermal models were applied: Langmuir (Mohanta & Ahmaruzzaman 2018) and Freundlich (Jiang *et al.* 2014).

The Langmuir isothermal equation for adsorption describes monolayer adsorption on a uniform surface and is expressed as follows:

$$\frac{c_e}{q_e} = \frac{1}{q_m \times k} + \frac{c_e}{q_m} \tag{6}$$

The Freundlich isothermal equation for adsorption describes non-ideal adsorption on a non-uniform surface and is expressed as follows:

$$q_e = k_f \times C_e^{1/n} \tag{7}$$

where q_e is the adsorption capacity at equilibrium (mg/g), c_e is the phosphate concentration at equilibrium (mg/L), q_m represents the maximum adsorption capacity (mg/g), k is the Langmuir constant, k_f is the Freundlich adsorption rate constant, and n is the adsorption intensity constant.

RESULTS AND DISCUSSION

Characteristics of YGs and CMYGs

The surface characteristics of the materials were extensively studied by using SEM/energy-dispersive X-ray spectroscopy (EDS) (Supplementary Material, SM, Figure S1, available with the online version of this paper). The SEM images showed that with increasing synthesis temperature of YGs and CMYGs, the number of irregular mesoporous structures increased, and the distribution of irregular mesoporous structures shifted from ordered to disordered (Yang *et al.* 2018). These irregular pore structures provided surface areas where considerable numbers of nanoparticles were present (Fang *et al.* 2014). The analysis of atomic mass ratio is displayed in Table 1. According to the results, the main composition elements of YGs were C and O, the sum of which accounted for more than 90%. After modification, the content of C in CMYGs was decreased, whereas the contents of Ca^{2+} and Mg^{2+} were increased, which were 0.06–0.63 and 10.37–23.22 times higher,

Table 1 | Elemental analysis of biochar at different carbonization temperatures

biochar		Element (%)								S_{BET} (m^2/g)	S_{micto} (m^2/g)	S_{ext} (m^2/g)	V_{tot} (cm^3/g)	V_{mic} (cm^3/g)	V_{ext} (cm^3/g)	D_p(nm)
		C	N	O	P	S	Si	Ca	Mg							
YGs	YG350	70.74	0.00	22.24	1.26	1.10	4.05	0.36	0.23	1.98	1.33	0.65	0.01	0.01	0.00	10.22
	YG550	84.03	0.00	13.21	0.21	0.71	1.28	0.16	0.41	5.01	0.36	4.64	0.01	0.01	0.00	7.77
	YG750	88.61	0.00	8.17	0.83	0.70	1.05	0.24	0.38	210.96	188.76	41.20	0.12	0.09	0.02	2.09
CMYGs	CMYG350	67.22	0.00	24.56	0.61	0.12	1.31	0.61	5.57	1.94	0.78	1.16	0.00	0.00	0.00	9.32
	CMYG550	82.16	0.00	10.52	0.37	0.50	1.66	0.17	4.62	7.08	4.02	3.06	0.01	0.01	0.00	6.96
	CMYG750	84.98	0.00	8.27	0.34	0.61	1.09	0.39	4.32	44.12	39.12	5.00	0.03	0.02	0.00	2.72

S_{BET}: Total specific surface area; S_{micto}: Micropore surface area; S_{ext}: External pore surface area; V_{tot}: Total pore volume; V_{mic}: Micropore volume; V_{ext}: External pore volume; D_p(nm): Pore diameter.

respectively, than those in YGs. These results indicated that some C elements on the CMYGs surface were covered by Ca^{2+} and/or Mg^{2+} and that Mg^{2+} was more effectively loaded on the surface of biochar than was Ca^{2+} (Hou *et al.* 2016). The SEM and elemental analyses showed that the soaking modification method was able to effectively load Ca^{2+} and Mg^{2+} onto the CMYGs surface.

The BET and pore structure analysis results for the YGs and CMYGs revealed some of the important properties of the biochars. Table 1 shows that the surface area of CMYG750 was 210.96 m^2/g, which is lower than that reported for other adsorbents, such as hazelnut husk (1,092 m^2/g) but higher than that of corn straw biochar (61.0 m^2/g) (Imamoglu & Tekir 2008; Song *et al.* 2014). The D_p values were less than 20 nm for all the biochars, indicating that there were large numbers of micropores and mesopores on the surfaces of the YGs and CMYGs (Jung *et al.* 2016). In addition, with increasing carbonization temperature, $S_{BET,}$ S_{micto} and V_{tot} decreased, whereas D_p gradually increased. These results can be attributed to the addition of calcium-magnesium ions or calcium-magnesium oxides, which resulted in the destruction of the original pore structure and the blocking of internal micropores as well as the unblocking of mesopores and macropores in the biochar (Zhou *et al.* 2013).

The major functional groups of an adsorbent are commonly identified by using FTIR spectroscopy. As seen in Figure S2 in the SM (available online), there were four strong absorption peaks in the 4,000–400 cm^{-1} region, and the trends of the infrared spectra were approximately the same, indicating that the species of chemical functional groups on the surface of the CMYGs were not changed by modification with Ca^{2+} and Mg^{2+} (Michálekovárichveisová *et al.* 2017). However, the intensities of the four absorption peaks were different, indicating that the calcium and magnesium ions may have combined with the surface functional groups, thereby affecting the absorption peak intensity (Zhou *et al.* 2013).

The XRD patterns show that the diffraction peaks are sharp and complex, indicating that the formed amorphous products have a high crystallinity and low purity (SM, Figure S2) (Zhou *et al.* 2013; Dawood *et al.* 2017). The XRD diffraction peaks of CMYG750 are similar to those of YG750, indicating that the calcium-magnesium oxides in the samples occur in an amorphous state (Li *et al.* 2016a). According to the results obtained with Jade 5.0, a strong diffraction peak appears near $2\theta = 25°$, which represents SiO_2 crystal based on comparison with the standard card (Zhou *et al.* 2013). Figure S2 shows several new peaks near $2\theta = 20°$, 40°, and 70° after the modification, indicating the presence of $Mg(OH)_2$ and MgO (Fang *et al.* 2014; Li *et al.* 2016b; Li *et al.* 2017). In addition, the XRD pattern analysis does not show the obvious characteristic peaks of CaO and $Ca(OH)_2$, which may be due to the low loading and small particle sizes or the overlapping with the characteristic peaks of calcium and magnesium oxide (Table 1).

Effect of the pH and carbonization temperature on phosphate removal

As shown in Figure 1, an experiment was conducted in the pH range from 4 to 10. The biochar adsorption capacity for phosphate increased with the increase in carbonization temperature, indicating that the final carbonization temperature had a large influence on the phosphate removal of biochar in the tested range. The amount of phosphate adsorbed by the YGs and CMYGs increased as the pH increased from 4 to 9 and then decreased.

Under our experimental conditions, phosphate predominantly existed in the anionic forms of HPO_4^{2-} or $H_2PO_4^-$ over the pH range of 4.0 to 10.0 (Figure 1). The MgO on the biochar surface was expected to be positively charged under the experimental aqueous conditions due to the point of zero charge (PZC) of MgO and $Mg(OH)_2$ at around 12 (Li *et al.* 2017) and was expected to exhibit strong affinity for negatively charged phosphate at lower pH values. For CMYGs, in solution of lower initial pH, the presence of Mg oxides would be protonated to $MgOH^+$, and surface electrostatic attraction between phosphate ions and protonated $MgOH^+$ would be expected (Yao *et al.* 2013; Li *et al.* 2017). The reaction can be simply

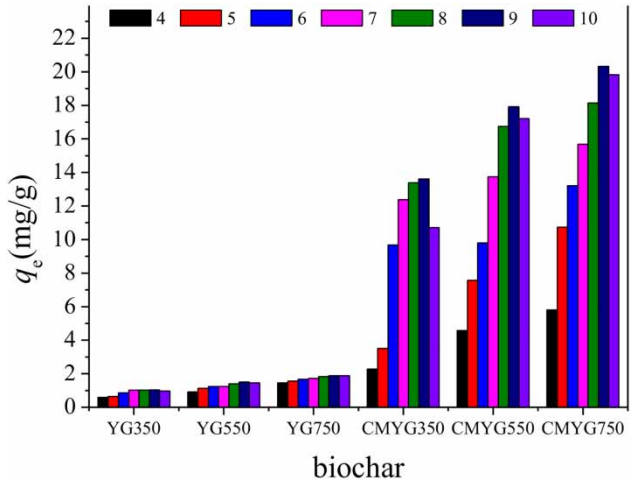

Figure 1 | Effect of the solution pH on YGs and CMYGs adsorption of phosphate.

described as follows at pH < 9.0:

$$\equiv MgO + H_2O \rightarrow \equiv MgOH^+ + OH^-;$$
$$Mg\text{-}OH^+ + H_2PO_4^- \rightarrow Mg\text{-}OH^+ - H_2PO_4^-;$$
$$Mg\text{-}OH^+ + HPO_4^{2-} \rightarrow Mg\text{-}OH^+ - HPO_4^{2-}$$

However, the $Mg\text{-}OH^+$ on the biochar was gradually occupied over time, and the above reaction rate with phosphate could gradually be slow down (Li *et al.* 2016b). At pH > 9.0, the increased OH^- concentration could not only compete for adsorption sites with phosphate, but also precipitate calcium and magnesium to block the pore of biochar (Zhou *et al.* 2013). Moreover, the previous study revealed that, when solution pH > pH_{pzc}, the surface of the modified biochar was negative (Chen *et al.* 2012). In this study, the pH_{pzc} of the CMYGs was 8.78, which was less than solution pH, indicating that the electrostatic repulsion between phosphate and the biochar may occur, and this consequently resulted in poor phosphate adsorption (Yang *et al.* 2018). Therefore, the maximum capacities of YGs and CMYGs to phosphate were obtained at pH 9.0.

Adsorption kinetics

Adsorption kinetics are typically used to estimate the rate of adsorption, which is an important characteristic used to measure the adsorption performance of an adsorbent (Li *et al.* 2018). The phosphate adsorption kinetics of YGs and CMYGs are shown in Figure S3 in the SM, available online). Although the time to reach phosphate adsorption saturation on the YGs and CMYGs was not consistent, all the materials reached the adsorption equilibrium within 50–100 min.

In this study, the phosphate adsorption kinetics data for the YGs and CMYGs were fitted with the three models. The fitting results in Table 2 show that the adsorption of phosphate by the YGs/CMYGs is best fitted by the pseudo-second-order kinetic model ($R^2 = 1$), which indicates that the phosphate adsorption on the biochars was conducted through the inner sphere complex (Li *et al.* 2017). The formation of chemical bonds is the main factor affecting the pseudo-second-order kinetics of adsorption (Jung *et al.* 2015; Yang *et al.* 2018). To determine the actual rate-controlling step, the kinetic data were fitted using an intraparticle diffusion equation (SM, Figure S4, available online). The curve of the intraparticle diffusion model showed that phosphate adsorption on the YGs/CMYGs occurred in multiple segments. In the first stage, the slope was high, and the adsorption capacity rapidly increased. In the second stage, the slope was lower, and the adsorption sites on the adsorbent decreased until the adsorption equilibrium was reached (Hou *et al.* 2016). The particle diffusion fitting equation of the YGs/CMYGs did not pass through the origin, which indicated that the phosphate adsorption process was also influenced by particle internal diffusion action (Zhang *et al.* 2013); thus, the process may be jointly controlled by surface adsorption and intraparticle diffusion (Li *et al.* 2017). As seen in Table 2, k_{p1} is greater than k_{p2}, and C_1 is lower than C_2, indicating that the phosphate removal rate is higher in the initial stage for biochar with a large specific surface area (Table 1). As adsorption continues, the boundary layer of biochar gradually forms, and the adsorption capacity is gradually lost (Hou *et al.* 2016). Thereafter, the adsorption rate is mainly determined by the rate at which the adsorbate is transported from the outside of the particle into the particle (Yang *et al.* 2018).

Adsorption isotherms

The biochar equilibrium adsorption capacity was increased with the temperature increasing (SM, Figure S5, available online), and the adsorption of YGs/CMYGs to phosphate was an endothermic process (Hou *et al.* 2016).

As can be seen from Table 3 and Figure S5, the *1/n* was lower than 1, suggesting the existence of a high adsorption intensity (Karunanithi *et al.* 2017). The q_m and b were

Table 2 | Kinetic parameters of the adsorption models

			1st-order			2nd-order				Piratical-order					
Biochar		$q_{e,exp}$ (mg/g)	k_1(min)	q_e (mg/g)	R^2	k_2 (g/kg/min)	q_e (mg/g)	R^2	h (g/mg/min)	k_{p1}	C_1	R_1^2	k_{p2}	C_2	R_2^2
YGs	YG 350	2.74	0.01	1.53	0.93	0.92	2.81	1.00	0.14	0.35	−0.22	0.95	0.04	1.77	0.85
	YG 550	2.92	0.01	1.90	0.86	0.88	2.90	1.00	0.14	0.39	−0.25	0.92	0.04	2.06	0.98
	YG 750	3.01	0.00	1.64	0.81	0.79	2.99	1.00	0.14	0.46	−0.43	0.94	0.03	2.24	0.97
CMYGs	CMYG350	34.50	0.01	11.14	0.87	0.00	35.71	1.00	5.10	7.95	−3.73	0.95	0.22	29.79	0.93
	CMYG550	76.60	0.01	35.16	0.93	0.00	83.33	1.00	7.81	14.12	−7.74	1.00	0.50	66.05	0.95
	CMYG750	81.10	0.01	45.50	0.97	0.00	90.91	1.00	5.88	16.60	−15.24	0.99	0.78	65.55	0.89

Table 3 | Phosphate adsorption isotherm parameter of YGs and CMYGs

			Langmuir			Freundlich		
Biochar		***T*(K)**	q_m(mg/g)	***b*(L/mg)**	R^2	k_f(mg/g(1/mg)$^{1/n}$)	1/*n*	R^2
YGs	YG350	288	1.83	0.010	0.94	0.01	0.90	0.96
		303	2.00	0.012	0.95	0.06	0.66	0.97
		318	2.10	0.016	0.96	0.07	0.63	0.97
	YG550	288	3.40	0.018	0.93	0.02	0.82	0.95
		303	3.68	0.021	0.94	0.05	0.77	0.98
		318	4.34	0.021	0.95	0.06	0.76	0.97
	YG750	288	4.63	0.018	0.95	0.01	0.946	0.95
		303	5.30	0.018	0.95	0.04	0.78	0.97
		318	6.54	0.023	0.97	0.26	0.42	0.98
CMYGs	CMYG350	288	14.71	0.022	0.94	0.07	0.88	0.97
		303	15.63	0.024	0.95	0.44	0.67	0.96
		318	22.22	0.025	0.96	0.77	0.66	0.98
	CMYG550	288	19.23	0.013	0.95	0.64	0.59	0.96
		303	55.56	0.014	0.97	1.46	0.55	0.95
		318	66.67	0.014	0.96	4.15	0.59	0.95
	CMYG750	288	62.50	0.018	0.94	1.68	0.77	0.97
		303	71.11	0.020	0.95	2.31	0.66	0.99
		318	90.91	0.022	0.97	3.87	0.42	0.99

increased with the rise in temperature, indicating that the adsorption rate and adsorption equilibrium capacity to phosphate of YGs/CMYGs were increased with the temperature increasing (Hou *et al.* 2016). The adsorption to phosphate of YGs/CMYGs were well fitted to the Freundlich ($R^2 > 0.95$) and Langmuir model ($R^2 > 0.94$). This finding indicates that in the absorption to phosphate of YGs/CMYGs with a single molecular layer and multimolecular layer adsorption, numerous inequality and uniform surfaces are present in the biochar surface, and adsorption may involve a variety of interactive relationships between the absorbent and the adsorbate. Besides, the maximum adsorption capacities of YG750 and CMYG750 to phosphate were 2.55 and 90.91 mg/g, respectively, and calcium-magnesium modification could enhance the adsorption capacities of CMYGs.

Adsorption mechanism

To further explore the mechanisms of phosphate adsorption by the CMYGs, the CMYG750 samples before and after phosphate adsorption (P-CMYG750) were characterized by FTIR spectroscopy and XRD analysis (Figure 2). In general, the FTIR broad band centered around 3,428 cm^{-1}

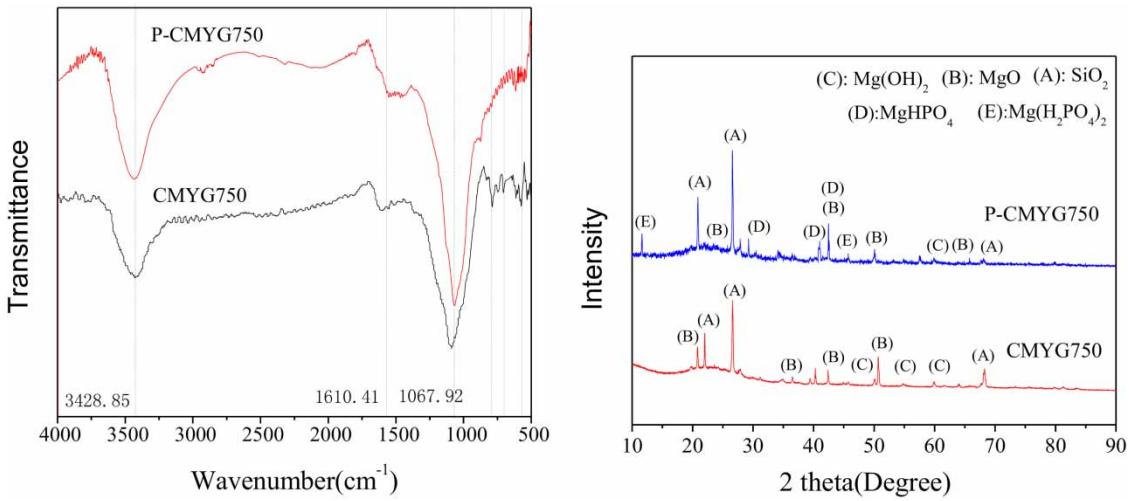

Figure 2 | FTIR and XRD analyses of CMYG750 and P-CMYG750.

was associated with the –OH stretching vibrations of the hydroxyl groups in the $Mg(OH)_2$ or the sorbed water molecules, and the peak located around 1,610 cm^{-1} was recorded as water deformation (Li *et al.* 2016b). The peaks around 900–1,000 cm^{-1} were assigned to the stretching and bending vibrations of Mg–O and Mg–OH (Li *et al.* 2016b). Furthermore, the peak around 500 cm^{-1} was assigned to Mg–O bond stretching vibrations (Yao *et al.* 2013; Li *et al.* 2017). After phosphate adsorption, the peaks around 900 cm^{-1} visible in the FTIR spectroscopy of the CMYG750 biochar corresponding to Mg–OH vibrations had largely disappeared, with a strengthening of the asymmetric vibrations of P–O bonds at around 1,067 cm^{-1} (Li *et al.* 2016b), implying the interaction between the Mg–OH group and phosphate ions and the possible formation of a surface inner-sphere complex (Yang *et al.* 2018). Compared with the Mg–O vibration peak around 500 cm^{-1} before phosphate adsorption, the peak around 500 cm^{-1} was decreased but still could be easily observed after phosphate adsorption, which indicated that the Mg–O group was also dedicated to the phosphate ion adsorption (Yao *et al.* 2013; Li *et al.* 2016b). However, the small change in the Mg–O peak around 500 cm^{-1} from before to after phosphate sorption suggests the formation of only new outer-sphere surface complexes between surface MgO and phosphate (Li *et al.* 2016b; Yang *et al.* 2018). The XRD analysis provided additional evidence of phosphate interactions with CMYG750 biochar upon sorption (Sahota *et al.* 2017). The P-CMYG750 exhibited strong signals of not only the existence of MgO and $Mg(OH)_2$ but also new crystals in the forms of $Mg(HPO_4)_2$ and $MgHPO_4$, which clearly indicated the precipitations between phosphate ions and Mg oxide (Li *et al.* 2016b; Li *et al.* 2017; Yang *et al.* 2018).

Therefore, based on the results of the kinetic and pH analyses, we propose that the phosphate adsorption was controlled by the combined processes of surface electrostatic attraction, inner-sphere complexation and precipitation (Li *et al.* 2017; Yang *et al.* 2018). Under our experimental conditions, phosphate predominantly existed in the anionic forms of HPO_4^{2-} and $H_2PO_4^-$ over the pH range of 4.0 to 10.0 (Li *et al.* 2017). During the initial stages of the adsorption experiment, surface electrostatic attraction between phosphate ions and protonated $MgOH^+$ would be expected (Jiang *et al.* 2014; Li *et al.* 2016b). As the reaction continued, precipitation between phosphate ions and Mg oxide particles on carbon surfaces within the matrix would have taken place, resulting in the formation of $Mg(HPO_4)_2$ and $MgHPO_4$ crystals (Bao *et al.* 2014; Li *et al.* 2016b).

Desorption

An ideal adsorbent is not only highly effective but can also easily desorb and maintain high adsorption efficiency after recycling. In this study, the P-CMYGs desorbed by pure water, 0.1 mol/L HCl, 0.1 mol/L NaOH or 0.1 mol/L NaCl were separated from the solution and washed with ultrapure water until neutral for recycling (SM, Figure S6, available online) (Yang *et al.* 2018). The removal rate of phosphate by CMYGs desorbed with water, 0.1 mol/L NaOH and 0.1 mol/L NaCl was unsatisfactory, and their values did not exceed 40% after five recycling. The low removal efficiency may have been due to the strong coordination and complexation between the magnesium ions on the surface of the biochar and the phosphate ions (Hou *et al.* 2016; Li *et al.* 2016b). Meanwhile, this result also indicated that there were some attractive sites that were not completely reversed during desorption (Hou *et al.* 2016; Li *et al.* 2016b; Yang *et al.* 2018). While the 0.1 mol/L HCl was used as the desorbent, the phosphate removal capacity by P-CMYG350, P-CMYG550 and P-CMYG750 decreased from 79.65%, 81.33% and 85.38% to 50.75%, 51.93% and 53.85%, respectively. The results showed that, as compared to the other desorbents, the 0.1 mol/L HCl was found to be the best one, and such a desorbent could only dissolve few of the coated materials of Ca and Mg (i.e. less than 0.1%), after 24 h processing. Meanwhile, the phosphate removal efficiency of the modified biochar desorbent by 0.1 mol/L HCl would be always higher than that of the other desorbents after five successive recycles. These results suggested that Ca and Mg have been located deep inside and strongly attached to the adsorbents. The findings demonstrated that CMYGs are the promising adsorbents for phosphate removal with high reusability.

CONCLUSIONS

The results demonstrated that MgO and $Mg(OH)_2$ were successfully deposited on the carbon surface within the biochar matrix, and the CMYGs showed strong ability to adsorb phosphate in aqueous solutions. The adsorption followed the pseudo-second-order models, and the equilibrium was achieved within 100 min. The equilibrium data were well described by the Freundlich and Langmuir models, and the maximum phosphate adsorption capacity of CMYG750 was 90.91 mg/g at pH 9.0. The CMYGs retained over 50% phosphate removal efficiency, after five successive recycles. The phosphate sorption mechanisms

involved surface electrostatic attraction, inner-sphere complexation and precipitation reactions. The results demonstrated CMYG750 is a promising adsorbent for environmental cleanup, particularly for the phosphate removal from wastewater.

ACKNOWLEDGEMENTS

This work was supported by the National Key Research and Development Program of China (2017YFD0801004) and the National Science and Technology Support Program of China (2010BAD03B03).

The authors have declared no conflict of interest.

REFERENCES

Babic, B. M., Milonjic, S. K., Polovina, M. J. & Kaludierovic, B. V. 1999 Point of zero charge and intrinsic equilibrium constants of activated carbon cloth. *Carbon* **37** (3), 477–481.

Bao, X., Qiang, Z., Chang, J. H., Ben, W. & Qu, J. 2014 Synthesis of carbon-coated magnetic nanocomposite (Fe_3O_4@C) and its application for sulfonamide antibiotics removal from water. *Journal of Environmental Sciences* **26** (5), 962–969.

Boparai, H. K., Joseph, M. & O'Carroll, D. M. 2011 Kinetics and thermodynamics of cadmium ion removal by adsorption onto nano zerovalent iron particles. *Journal of Hazardous Materials* **186** (1), 458–465.

Chen, N., Feng, C. P., Zhang, Z. Y., Liu, R. P., Gao, Y., Li, M. & Sugiura, N. 2012 Preparation and characterization of lanthanum(III) loaded granular ceramic for phosphorus adsorption from aqueous solution. *Journal of the Taiwan Institute of Chemical Engineers* **43** (5), 783–789.

Cordell, D., Rosemarin, A., Schroder, J. J. & Smit, A. L. 2011 Towards global phosphorus security: a systems framework for phosphorus recovery and reuse options. *Chemosphere* **84** (6), 747–758.

Dawood, S., Sen, T. K. & Phan, C. 2017 Synthesis and characterization of slow pyrolysis pine cone bio-char in the removal of organic and inorganic pollutants from aqueous solution by adsorption: kinetic, equilibrium, mechanism and thermodynamic. *Bioresource Technology* **246**, 76–81.

Elser, J. & Bennett, E. 2011 A broken biogeochemical cycle. *Nature* **478** (7367), 29–31.

Fang, C., Zhang, T., Li, P., Jiang, R. F. & Wang, Y. C. 2014 Application of magnesium modified corn biochar for phosphorus removal and recovery from swine wastewater. *International Journal of Environmental Research and Public Health* **11** (9), 9217–9237.

Fox, S., Oren, Y., Ronen, Z. & Gilron, J. 2014 Ion exchange membrane bioreactor for treating groundwater contaminated with high perchlorate concentrations. *Journal of Hazardous Materials* **264** (2), 552–559.

Guo, Y. J., Tang, H., Li, G. D. & Xie, D. T. 2014 Effects of Cow dung biochar amendment on adsorption and leaching of nutrient from an acid yellow soil irrigated with biogas slurry. *Water Air and Soil Pollution* **225** (1820), 2–13.

He, X. M., Zhang, T., Ren, H. Q., Li, G. X., Ding, L. L. & Pawlowski, L. 2017 Phosphorus recovery from biogas slurry by ultrasound/H_2O_2 digestion coupled with HFO/biochar adsorption process. *Waste Management* **60**, 219–229.

Hou, J., Huang, L., Yang, Z. M., Zhao, Y. Q., Deng, C. R., Chen, Y. C. & Li, X. 2016 Adsorption of ammonium on biochar prepared from giant reed. *Environmental Science and Pollution Research* **23** (19), 19107–19115.

Imamoglu, M. & Tekir, O. 2008 Removal of copper (II) and lead (II) ions from aqueous solutions by adsorption on activated carbon from a new precursor hazelnut husks. *Desalination* **228** (1), 108–113.

Jiang, C., Jia, L., Zhang, B., He, Y. & Kirumba, G. 2014 Comparison of quartz sand, anthracite, shale and biological ceramsite for adsorptive removal of phosphorus from aqueous solution. *Journal of Environmental Sciences* **26** (2), 466–477.

Jung, K. W. & Ahn, K. H. 2016 Fabrication of porosity-enhanced MgO/biochar for removal of phosphate from aqueous solution: application of a novel combined electrochemical modification method. *Bioresource Technology* **200**, 1029–1032.

Jung, K. W., Jeong, T. U., Hwang, M. J., Kim, K. & Ahn, K. H. 2015 Phosphate adsorption ability of biochar/Mg-Al assembled nanocomposites prepared by aluminum-electrode based electro-assisted modification method with mgcl2 as electrolyte. *Bioresource Technology* **198**, 603–610.

Jung, K. W., Jeong, T. U., Kang, H. J., Chang, J. S. & Ahn, K. H. 2016 Preparation of modified-biochar from Laminaria japonica: simultaneous optimization of aluminum electrode-based electro-modification and pyrolysis processes and its application for phosphate removal. *Bioresource Technology* **214**, 548–557.

Karunanithi, R., Ok, Y. S., Dharmarajan, R., Ahmad, M., Seshadri, B., Bolan, N. & Naidu, R. 2017 Sorption, kinetics and thermodynamics of phosphate sorption onto soybean stover derived biochar. *Environmental Technology & Innovation* **8**, 113–125.

Li, R. H., Wang, J. J., Zhou, B. Y., Awasthi, M. K., Ali, A., Zhang, Z. Q., Gaston, L. A., Lahori, A. H. & Mahar, A. 2016a Enhancing phosphate adsorption by Mg/Al layered double hydroxide functionalized biochar with different Mg/Al ratios. *Science of the Total Environment* **559**, 121–129.

Li, R. H., Wang, J. J., Zhou, B. Y., Awasthi, M. K., Ali, A., Zhang, Z. Q., Lahori, A. H. & Mahar, A. 2016b Recovery of phosphate from aqueous solution by magnesium oxide decorated magnetic biochar and its potential as phosphate-based fertilizer substitute. *Bioresource Technology* **215**, 209–214.

Li, R. H., Wang, J. J., Zhou, B. Y., Zhang, Z. Q., Liu, S., Lei, S. & Xiao, R. 2017 Simultaneous capture removal of phosphate, ammonium and organic substances by MgO impregnated biochar and its potential use in swine wastewater treatment. *Journal of Cleaner Production* **147**, 96–107.

Li, S., Zeng, Z. & Xue, W. 2018 Adsorption of lead ion from aqueous solution by modified walnut shell: kinetics and thermodynamics. *Environmental Technology* DOI: 10.1080/09593330.2018.1430172.

Loganathan, P., Vigneswaran, S., Kandasamy, J. & Bolan, N. S. 2014 Removal and recovery of phosphate from water using sorption. *Critical Reviews in Environmental Science & Technology* **44** (8), 847–907.

Melia, P. M., Cundy, A. B., Sohi, S. P., Hooda, P. S. & Busquets, R. 2017 Trends in the recovery of phosphorus in bioavailable forms from wastewater. *Chemosphere* **186**, 381–395.

Michálekovárichveisová, B., Frišták, V., Pipíška, M., Ď, L., Morenojimenez, E. & Soja, G. 2017 Iron-impregnated biochars as effective phosphate sorption materials. *Environmental Science and Pollution Research* **24** (1), 463–475.

Mohanta, D. & Ahmaruzzaman, M. 2018 Bio-inspired adsorption of arsenite and fluoride from aqueous solutions using activated carbon@SnO_2 nanocomposites: isotherms, kinetics, thermodynamics, cost estimation and regeneration studies. *Journal of Environmental Chemical Engineering* **6** (1), 356–366.

Qiu, G. L., Law, Y. M., Das, S. & Ting, Y. P. 2015 Direct and complete phosphorus recovery from municipal wastewater using a hybrid microfiltration-forward osmosis membrane bioreactor process with seawater brine as draw solution. *Environmental Science & Technology* **49** (10), 6156–6163.

Rittmann, B. E., Mayer, B., Westerhoff, P. & Edwards, M. 2011 Capturing the lost phosphorus. *Chemosphere* **84** (6), 846–853.

Sahota, S., Vijay, V. K., Subbarao, P., Chandra, R., Ghosh, P., Shah, G., Kapoor, R., Vijay, V., Koutu, V. & Thakur, I. S. 2017 Characterization of leaf waste based biochar for cost effective hydrogen sulphide removal from biogas. *Bioresource Technology* **250**, 635–641.

Shi, Z. L., Liu, F. M. & Yao, S. H. 2011 Adsorptive removal of phosphate from aqueous solutions using activated carbon loaded with Fe(III) oxide. *New Carbon Materials* **26** (4), 299–306.

Song, Z., Lian, F., Yu, Z., Zhu, L., Xing, B. & Qiu, W. 2014 Synthesis and characterization of a novel MnO_x-loaded biochar and its adsorption properties for Cu^{2+} in aqueous solution. *Chemical Engineering Journal* **242** (242), 36–42.

Wan, S., Wang, S. S., Li, Y. C. & Gao, B. 2017 Functionalizing biochar with Mg-Al and Mg-Fe layered double hydroxides for removal of phosphate from aqueous solutions. *Journal of Industrial and Engineering Chemistry* **47**, 246–253.

Yang, Q., Wang, X. L., Luo, W., Sun, J., Xu, Q. X., Chen, F., Zhao, J. W., Wang, S. N., Yao, F. B., Wang, D. B., Li, X. M. & Zeng, G. M. 2018 Effectiveness and mechanisms of phosphate adsorption on iron-modified biochars derived from waste activated sludge. *Bioresource Technology* **247**, 537–544.

Yao, Y., Gao, B., Chen, J. J., Zhang, M., Inyang, M., Li, Y. C., Alva, A. & Yang, L. Y. 2013 Engineered carbon (biochar) prepared by direct pyrolysis of Mg-accumulated tomato tissues: characterization and phosphate removal potential. *Bioresource Technology* **138**, 8–13.

Yin, H. & Kong, M. 2014 Simultaneous removal of ammonium and phosphate from eutrophic waters using natural calcium-rich attapulgite-based versatile adsorbent. *Desalination* **351** (3), 128–137.

Zhang, M. & Gao, B. 2013 Removal of arsenic, methylene blue, and phosphate by biochar/AlOOH nanocomposite. *Chemical Engineering Journal* **226** (24), 286–292.

Zhang, M., Gao, B., Yao, Y., Xue, Y. & Inyang, M. 2012 Synthesis of porous MgO-biochar nanocomposites for removal of phosphate and nitrate from aqueous solutions. *Chemical Engineering Journal* **210** (4), 26–32.

Zhang, M., Gao, B., Yao, Y. & Inyang, M. 2013 Phosphate removal ability of biochar/MgAl-LDH ultra-fine composites prepared by liquid-phase deposition. *Chemosphere* **92** (8), 1042–1047.

Zhou, H., Jiang, Z. & Wei, S. 2013 A novel absorbent of nano-Fe loaded biomass char and its enhanced adsorption capacity for phosphate in water. *Journal of Chemistry* **2013** (4), 1–9.

Zhu, N. Y., Yan, T. M., Qiao, J. & Cao, H. L. 2016 Adsorption of arsenic, phosphorus and chromium by bismuth impregnated biochar: adsorption mechanism and depleted adsorbent utilization. *Chemosphere* **164**, 32–40.

First received 15 September 2018; accepted in revised form 21 December 2018. Available online 7 January 2019